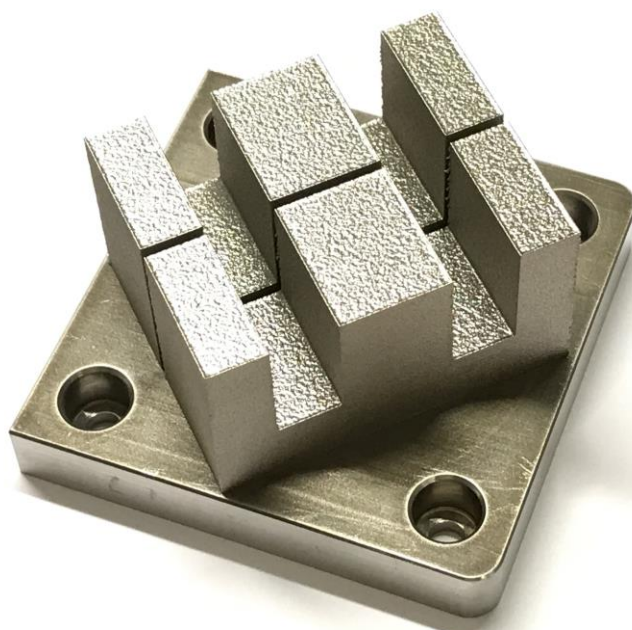


3D-printed high-frequency inductor for electric vehicles



Författare: Tag Hammam*, Peter Andersson*, Thord Nilson**, Lars Lindberg** and Hans Peter Nee***

*Swerim, **Inmotion technologies AB, ***KTH

Datum: 2021-05-26

Projekt inom "Elektronik, mjukvara och kommunikation - FFI - juni 2020"

FFI Fordonsstrategisk
Forskning och
Innovation

VINNOVA

Energimyndigheten

TRAFIKVERKET

FKG

VOLVO

SCANIA

VOLVO

SCANIA

VOLVO

SCANIA

VOLVO

SCANIA

VOLVO

Innehållsförteckning

1 Summary	4
2 Executive summary in English	4
3 Introduction	5
4 Experiments and Results	5
4.1 Sample preparation	5
4.2 Electric resistivity.....	6
4.3 Thermal measurements	10
4.4 Magnetic measurements.....	13
5 3D printed E-core	18
6 Discussions	20
6.1 Methods to reduce the eddy current	20
6.2 Material properties	21
7 Project goal	23
8 Results and goal fulfillment	23
9 Dissemination and publication	24
9.1 Dissemination of knowledge and results.....	24
9.2 Publikations	24
10 Conclusions and further research	24
11 Project participants and contact persons	24
12 Acknowledgments	24
13 References	25

Kort om FFI

FFI är ett samarbete mellan staten och fordonsindustrin om att gemensamt finansiera forsknings- och innovationsaktiviteter med fokus på områdena Klimat & Miljö samt Trafiksäkerhet. Satsningen innebär verksamhet för ca 1 miljard kr per år varav de offentliga medlen utgör drygt 400 Mkr.

För närvarande finns fem delprogram; Energi & Miljö, Trafiksäkerhet och automatiserade fordon, Elektronik, mjukvara och kommunikation, Hållbar produktion och Effektiva och uppkopplade transportsystem. Läs mer på www.vinnova.se/ffi.

1 Summary

To take advantage of the full performance of the new SiC switches, high-frequency passive components with low losses are needed. In this study, a 3D-printed soft magnetic material was evaluated, with the goal to reduce the size of inductors as well as reduce the electric loss. The target value of permeability was not reached but could still be used for an inductor. However, the losses were too high mainly due to the eddy current. There are three ways to reduce the eddy current that may be considered:

- 1) 3D printed internal structure, to break up the eddy current
- 2) Coat each powder-particle wither an insulating layer. The layer needs also act as a binder/adhesive to keep the inductor together
- 3) A laminated structure with insulating layer in-between each layer.

Based on the evaluation of 3D printed test samples of amorphous/nanocrystalline FeSiB type alloy, the following conclusions are due:

1. The present design with a solid core resulted in a too high eddy current.
2. The present type of alloy amorphous/nanocrystalline FeSiB type alloy may well result in both small size of the inductor and low losses, according to a reference [8].
3. Only one material (Fe-Ni-Mo, (product name MPP). was found in the literature that fulfilled the required properties of the soft magnetic material [9].

2 Executive summary in English

A transition to electric vehicles is underway, and the challenge is to reduce the battery cost for electric vehicles and at the same time increase the driving distance between charges. Therefore, small electrical losses as well as small, compact size of the electrical system (eg converters) are very important in electric vehicles. The cost of batteries today is about half the cost of an electric car, and therefore even quite expensive solutions to reduce electrical losses can be financially well justified.

The trend in power electronics is to replace silicon components with SiC components to increase efficiency and reduce the size of the system by increasing the electrical frequency. The implementation of SiC components in vehicles is the result of at least two decades of global research and development. However, increased frequency results in increased losses in passive components such as inductors and transformers, and these components are also difficult to cool. The electrical losses in inductors can be 3-4 times higher than the losses from the SiC components, and it also limits the frequency.

To take advantage of the full performance of the new SiC switches, high-frequency passive components with low losses are needed. In this study, a 3D-printed soft magnetic material was evaluated, with the goal to reduce the size of inductors as well as reduce the electric loss. The target value of permeability was not reached but could still be used for an inductor. However, the losses were too high mainly due to the eddy current. There are three ways to reduce the eddy current that may be considered:

- 1) 3D printed internal structure, to break up the eddy current
- 2) Coat each powder-particle wither an insulating layer. The layer needs also act as a binder/adhesive to keep the inductor together
- 3) A laminated structure with insulating layer in-between each layer.

Based on the evaluation of 3D printed test samples of amorphous/nanocrystalline FeSiB type alloy, the following conclusions are due:

1. The present design with a solid core resulted in a too high eddy current.
2. The present type of alloy amorphous/nanocrystalline FeSiB type alloy may well result in both small size of the inductor and low losses, according to a reference [8].
3. Only one material (Fe-Ni-Mo, (product name MPP). was found in the literature that fulfilled the required properties of the soft magnetic material [9].

3 Introduction

A transition to electric vehicles is underway, and the challenge is to reduce the battery cost for electric vehicles and at the same time increase the driving distance between charges. Therefore, small electrical losses as well as small, compact size of the electrical system (eg converters) are very important in electric vehicles. The cost of batteries today is about half the cost of an electric car, and therefore even quite expensive solutions to reduce electrical losses can be financially well justified.

The trend in power electronics is to replace silicon components with SiC components to increase efficiency and reduce the size of the system by increasing the electrical frequency. The implementation of SiC components in vehicles is the result of at least two decades of global research and development. However, increased frequency results in increased losses in passive components such as inductors and transformers, and these components are also difficult to cool. The electrical losses in inductors can be 3-4 times higher than the losses from the SiC components, and it also limits the frequency. To take advantage of the full performance of the new SiC switches, high-frequency passive components with low losses are therefore needed.

Exmet AB in Kista develops and licenses technology for additive manufacturing (3D printing) of amorphous and nanocrystalline metals. The focus of the development work has been on the development of processes and materials with soft magnetic properties

The aim with this study is to evaluate a 3D printed inductor with optimized soft magnetic materials.

4 Experiments and Results

The starting material for 3d printing was an amorphous FeSiB based powder. The test plan for evaluation of the 3D printed material as well eventual heat treatment was as follow:

1. 3D printing of test cylinders for measuring electric resistivity and thermal conduction

Three different material conditions were included:

- As printed - A
- Heat treatment B
- Heat treatment C

2. 3D printing of toroid for magnetic measurements

Three different material conditions were included:

- As printed - A
- Heat treatment B
- Heat treatment C

The electric resistivity and thermal conduction measurements as well as the magnetic measurement is presented in the text below.

4.1 Sample preparation

The 3D printing was performed in a laser-based powder bed fusion system. The system used was a M290 from EOS in Germany. The object was built on a base plate of stainless steel, and thereafter cut either in a precision cutting machine or in a wire electrical discharge machine (wire EDM). In the case of wire EDM was used, the surface was grinded/polished to remove the top surface that may have been affected by the electrical discharge process. An example of a 3D printed object used for magnetic measurements in this study is shown in

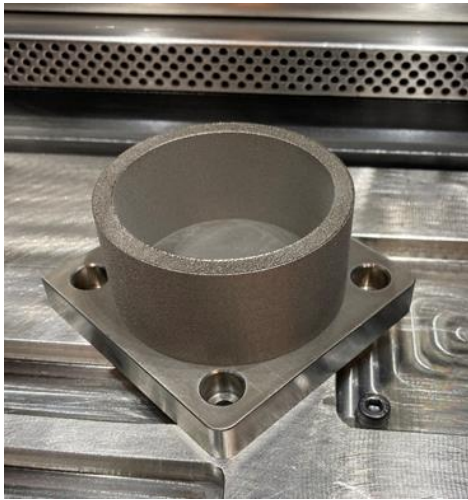


Figure 1. A 3D printed "tower" printed on a base plate made of stainless steel.



*Figure 1. A ring cut from the "tower" in **Error! Reference source not found.** by using a precision cutting machine*

4.2 Electric resistivity

The resistivity was measured by applying a DC current on the sample and thereafter the voltage drop at a section of the sample was measured. The prerequisite for an accurate measurement is that the current is evenly distributed at the section where the voltage drop measurements are performed.

For a long wire this is in general not a problem. For a short rod, however, there must be a sufficient length for the current to be evenly distributed over the cross-sectional area before the current reaches the part where the voltage drop is measured. In addition, a short length of the section which the voltage drop is measured will increase the measuring error. Therefore, a special fixture was made to be able to measure the resistivity of rods, see *Figure 2* and

Error! Reference source not found.. The voltage drop and current was measured with a digital multimeter (Keithley 2700), and the current source was a ripple free Kenwood P20. The presented voltage drop is the average value of the measured voltage drop at forward and reversed current.



Figure 2. A measuring fixture was made to be able to measure the resistivity of rods

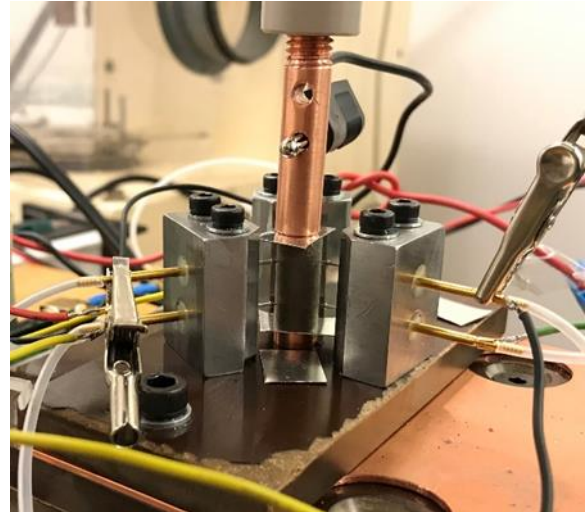


Figure 4. The voltage drop measurements was measured with three pairs of pneumatic probes. The distance between the two probes for all the three pairs of probes was 10.0 mm.

The voltage drop measurements was measured with three pairs of pneumatic probes. The distance between the two probes for all the three pairs of probes was 10.0 mm. At an evenly distributed current at the measuring sections, the deviations between the three pairs of probes should only depend on measuring error caused by the instruments or difference in the distance between two probes, which constitutes a pair of measuring probes. To estimate this error, measurement was performed on a relatively long rod (90 mm). Thereafter, measurements were made on copper rods of different length, see Table 1.

Table 1. Electric resistivity measurements of copper rods of different length. Measuring current: 10 A DC. Diameter of the rods: 10.0 mm. Copper: CW008A.

	Length (mm)	Min distance from probe to edge of sample (mm)	Resistivity ($\Omega \cdot \text{mm}^2/\text{m}$)	Temperature of test sample ($^{\circ}\text{C}$)	Estimated resistivity at 20 $^{\circ}\text{C}$ ($\Omega \cdot \text{mm}^2/\text{m}$)	Max deviation from mean value of one out of three probes (%)
Cu rod	90	20	0.0169	22	0.0167	3.5
Cu rod	90	20	0.0169	22	0.0168	4.7
Cu rod	90	20	0.0169	22	0.0168	2.4
Mean value			0.0169	22	0.0168	3.6
Cu rod	21	5.5	0.0169	22	0.0167	10.3
Cu rod	21	5.5	0.0170	22	0.0168	9.2
Mean value	21	5.5	0.0169	22	0.0168	9.8
Cu rod	18	4	0.0167	22	0.0166	11.1
Cu rod	18	4	0.0168	22	0.0167	12.9
Mean value	18	4	0.0167	22	0.0166	12.0
Cu rod	14	2	0.0172	22	0.0170	60.8
Cu rod	14	2	0.0169	22	0.0167	43.6
Mean value	14	2	0.0170	22	0.0169	52.2
Resistivity of CW008A at 20 C according to data sheet 0.0172						

The average max deviation from mean value of one out of three probes (%) was 3.6 % for the 90 mm long rod, and this value increased up to 52.2 % for the 14 mm long rod. The average resistivity for the 21 mm long rod was the same as for the 90 mm long rod. However, for rods shorter than 21 mm the measured average resistivity deviated from the measured value for the 90 mm long rod. Thus, with 10 mm distance between the measuring probes, the minimum length of a 10 mm diameter copper rod is 21 mm.

The electric resistivity was measured for five 3D printed rods (as-printed) with a length of 22 mm and a diameter of 10 mm, see Table 2. The current was 1 A Dc for all samples. The average value was 1.782 $\Omega\text{mm}^2/\text{m}$.

Table 2. The measured resistivity of five 3D printed rods (as-printed) with a length of 22 mm and a diameter of 10 mm. The alloy was an amorphous FeSiB type of alloy.

	Sample #	Resistivity ($\text{Ohm} \cdot \text{mm}^2/\text{m}$)	Max deviation from mean value of one out of three probes (%)
Mean value	1	1.737	14.7
	1	1.765	8.4
		1.751	11.6
Mean value	2	1.782	21.2
	2	1.791	25.7
		1.787	23.5
Mean value	3	1.786	14.9
	3	1.807	26.4
		1.797	20.7
Mean value	4	1.787	9.9
	4	1.788	21.4
		1.788	15.6
Mean value	5	1.762	
	5	1.813	12.8
		1.788	23.6
		18.2	
Mean value of all		1.782	

Measurements were also performed on a part of a ring (outer diameter: 64 mm, inner diameter 54 mm, thickness 3 mm). A pair of probes with 10 mm distance was used to measure the voltage drop. The voltage drop was measured at the outer edge, inner edge and in the middle of the ring. The measurements for the rings are presented in Table 3.

Table 3. The measured resistivity of an 3D printed ring, made of an FeSiB type of alloy.

	Position of the measuring probes		Resistance Ohm	Resistivity (Ohm*mm ² /m)
Mean value	inner circle		0.0032	4.050
	inner circle		0.0032	
	inner circle		0.0032	
Mean value	in the middle of the ring		0.0032	3.894
	in the middle of the ring		0.0029	
	in the middle of the ring		0.0031	
Mean value	outer circle		0.0024	3.259
	outer circle		0.0028	
	outer circle		0.0026	
Total mean value				3.734

The maximum measured resistivity was measured at the inner edge of the ring, and the minimum measured resistivity was measured at the outer edge of the ring. This is probably due to that the current density increases from the outer edge of the ring and reaches a maximum at the inner edge of the ring, which in turn is due to that the travel distance for the current is reduced at the inner edge.

The same type of ring was also measured by Inmotion. The average measurements of the rings and the 22 mm rod, all as printed is presented in **Error! Reference source not found.** The difference between Swerim's and Inmotion's value of resistivity is quite small. However, the discrepancy between the measured value of the rings and the rod is quite large.

4.3 Thermal measurements

Thermal conductivity describes the ability of a material to conduct heat, and the specific heat capacity, C_p , tells how much heat energy is absorbed or released depending on the temperature difference and mass. The thermal diffusivity, Δ , is a measure of transient heat-flow and is defined as the thermal conductivity, K , divided by the product of the specific heat, C_p , times the density, ρ : $\Delta=K/(C_p \rho)$.

The Transient Plane Source method

The Transient Plane Source (TPS) method (even known as the Hot Disk method) was used to measure the Thermal Conductivity and Specific Heat Capacity. Thermal Conductivity and Diffusivity are tested directly, and Specific Heat calculated from the former two. The TPS method requires one or two pieces of the sample in question to test, each needing no more than one flat surface where the Hot Disk double spiral sensor can be applied to.

The thermal conductivity measurements were performed according to the description in manual by using (Hot Disk) TPS 2500S, which is shown in Figure 3, by using the slab module software with standard analysis and using supplied values of temperature coefficient of resistance.

The sensor which was used was type 8563 with a 25 μm Kapton insulating coating and a radius of 3.189 mm of the sensor element. The sensor element was of nickel foil type F1. The sensor consists of a double spiral nickel and the sensor is sandwiched between two flat surfaces of the plates of each alloy. The thermal resistance between sensor and plates or samples was reduced by using glycerol and that expand somewhat the range of time or the first data point used in the analysis. The thermal conductivity accuracy is better than 5 %, according to the specification of the instrument.

The instrument is shown in Figure 3 and the sample holder is shown in Figure 4. Glycerol was used to reduce thermal contact between sensor and specimens of each alloy.



Figure 3. TPS 2500 S equipment.



Figure 4. Sample holder with two rods and the sensor clamped in between (the arrow points at the sensor).

The thermal conductivity was measured during a very slow heat ramp, from 20 $^{\circ}\text{C}$ to 200 $^{\circ}\text{C}$ during 16 hours. The measurement should ideally be measured during constant temperature (isothermal). However, measurement during a heat ramp will reveal eventually phase transformation, as initial measurements had indicated.

The measured thermal conductivity at a temperature from 20 $^{\circ}\text{C}$ up to 200 $^{\circ}\text{C}$ is presented in Figure 5 and in Table 4. In Table 5 the measured thermal conductivity for both as-printed and Heat treated sample (Heat treatment B) is presented. The thermal conductivity is somewhat improved with heat treatment.

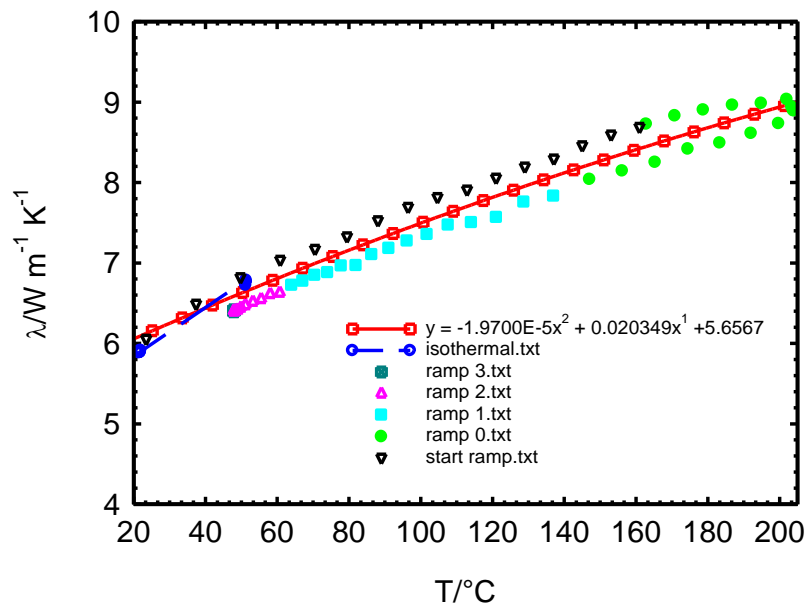


Figure 5. The measured thermal conductivity λ (W/m K) at a temperature from 20 °C up to 200 °C. Test sample – as printed.

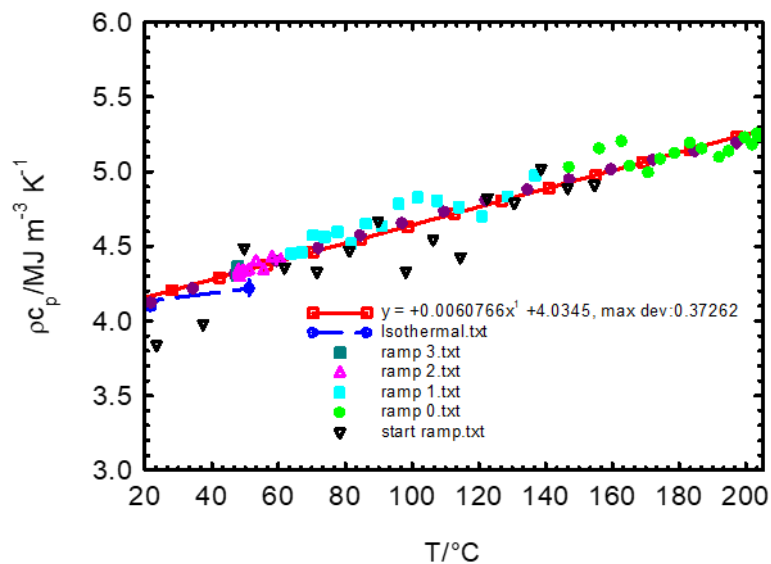


Figure 6. The estimated specific heat capacity at a temperature from 20 °C up to 200 °C. Test sample – as printed.

Table 4. The estimated thermal conductivity λ (W/m K) at a temperature from 20 °C up to 200 °C
Test samples – as printed and Heat treatment B

Temperature °C	Thermal Conductivity W/(m K) as printed	Thermal Conductivity W/(m K) Heat treatment B
20	6.1	6.8
29	6.2	7.0
38	6.4	7.1
47	6.6	7.3
56	6.7	7.4
65	6.9	7.6
74	7.1	7.8
83	7.2	7.9
92	7.4	8.1
101	7.5	8.2
110	7.7	8.4
119	7.8	8.5
128	7.9	8.7
137	8.1	8.8
146	8.2	9.0
155	8.3	9.1
164	8.5	9.3
173	8.6	9.4
182	8.7	9.6
191	8.8	9.7
200	8.9	9.9

4.4 Magnetic measurements

Scope

Test of magnetic properties of some samples of 3D printed amorphous material that is intended for high frequency inductors and transformers.

Desired properties of material

- dB/dt between 0.1 T/μs to 0.2 T/μs without excessive losses.
- Saturation flux minimum 0.3 T
- Saturation flux preferred > 0.6 T
- Permeability minimum 500
- Permeability preferred > 1000

Test samples and setup

Three samples with the following dimensions has been tested:

Sample	ϕ_i (mm)	ϕ_y (mm)	Thickness (mm)	Effective area (mm ²)	Effective length (mm)
A9 Untreated	54	64	3.20	16.0	185.3
B9 Heat Treated B	54	64	2.50	12.5	185.3
C9 Heat Treated C	54	64	2.51	12.55	185.3

The materials B9 and C9 are treated to see what improvement in magnetic properties can be obtained. A9 is untreated and is as coming directly from the 3D printer.



Figure 7. Typical Sample to the left and sample with windings to the right.

Typical Samples are presented in Figure 7. Two 30 turn windings with ϕ 1mm cu wire for excitation and one thinner 30 turn winding for measurement was added.

Test results

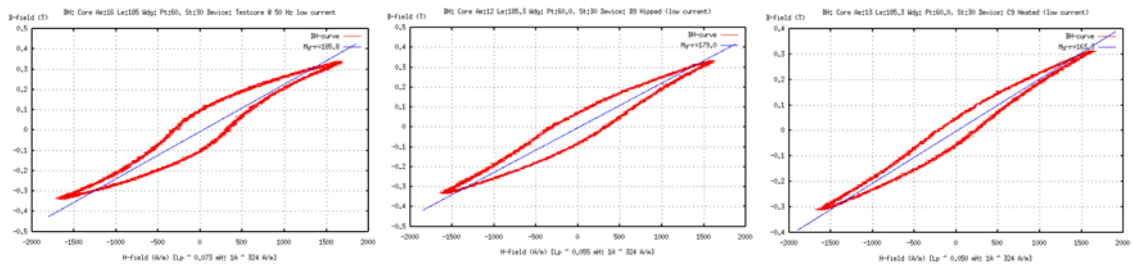
Testing at 50Hz

Testing was performed at three different current levels, low current at about 10A peak-peak, medium current at about 25A peak-peak and high current at about 115-120A peak-peak. At this frequency it is assumed that the effects of eddy currents can be ignored. To verify this the C9 sample was also tested at 10 and 20 Hz with the low current and the result was that the coercivity increased a bit.

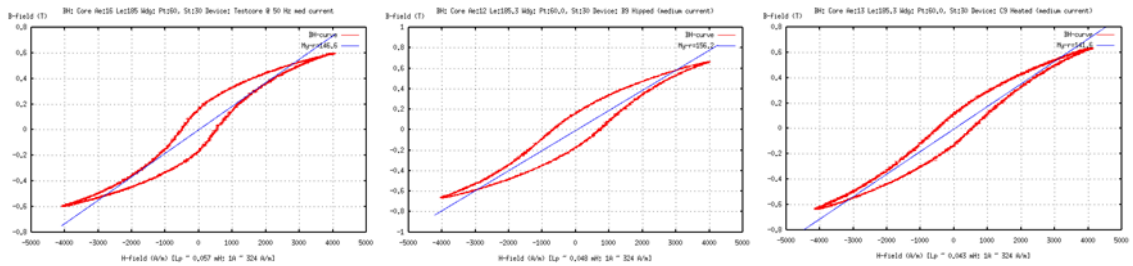
The figures below show the BH-curve, also called hysteresis loop of the material.

The material A9 in the figure to the left, B9 in the middle and C9 to the right.

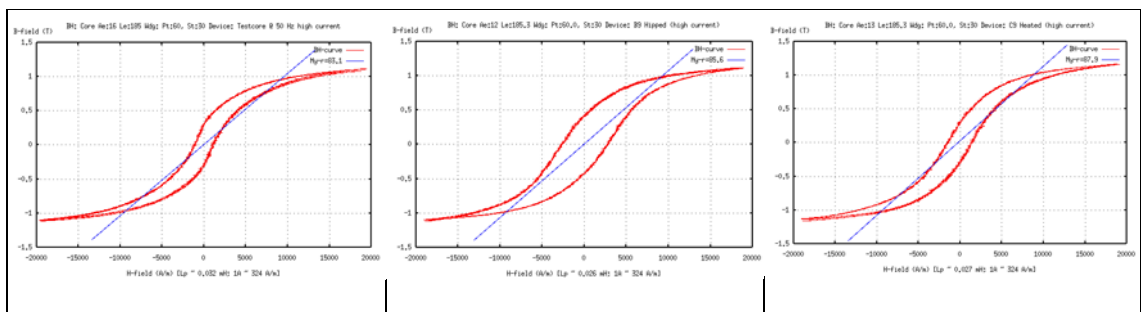
The permeability is calculated using 80% of the peak-flux in each figure and the result is shown in the blue line.



At a flux of about 0.3T the effective permeability is between 163 and 186.



Going up to peak about 0.6T the permeability drops to around 150.



Saturation occurs at around 1T. The permeability is too low for the material to be suitable for transformer usage. It is still suitable for an inductor; however, the hysteresis losses are also quite high which will result in high losses at high frequencies.

Summary of material properties in the table below.

Sample	Low current	Medium current	High current
A9 – Permeability	186	146	84
B9 – Permeability	179	156	86
C9 – Permeability	163	142	88
A9 – Coercivity (A/m)	313	522	1101
B9 – Coercivity (A/m)	320	699	2707
C9 – Coercivity (A/m)	227	514	1433

No significant improvement of magnetic properties can be seen due to Heat-treatment. The most notably difference is that the coercivity increased for the B9 and C9 samples at high current.

The hysteresis losses are proportional to the area inside the hysteresis loop, it may therefore be beneficial to compare to a commercially available material. A curve for a such material is shown in Figure 8.

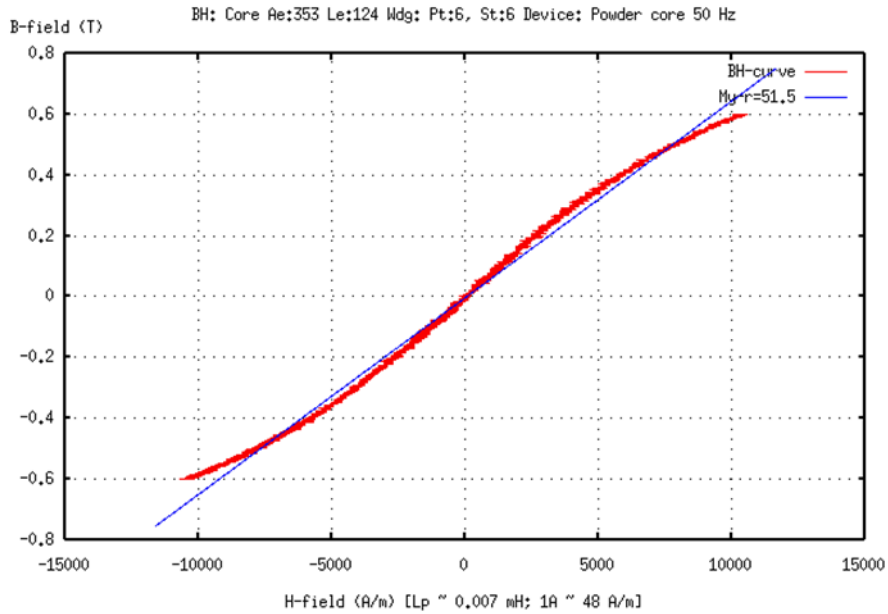


Figure 8. Measured hysteresis loop of a commercially available material, the hysteresis losses are relatively small.

Testing at higher frequencies

The figure below (Figure 9) shows the BH-curve for A9 obtained at 20 kHz. As can be seen the curve is quite different, this is because of eddy currents. With a H-field of 15000A/m we get less than 0.7T at 20 kHz, but at 50Hz we get slightly more than 1T. The difference is because of eddy currents in the material generating an opposing field and also significant losses.

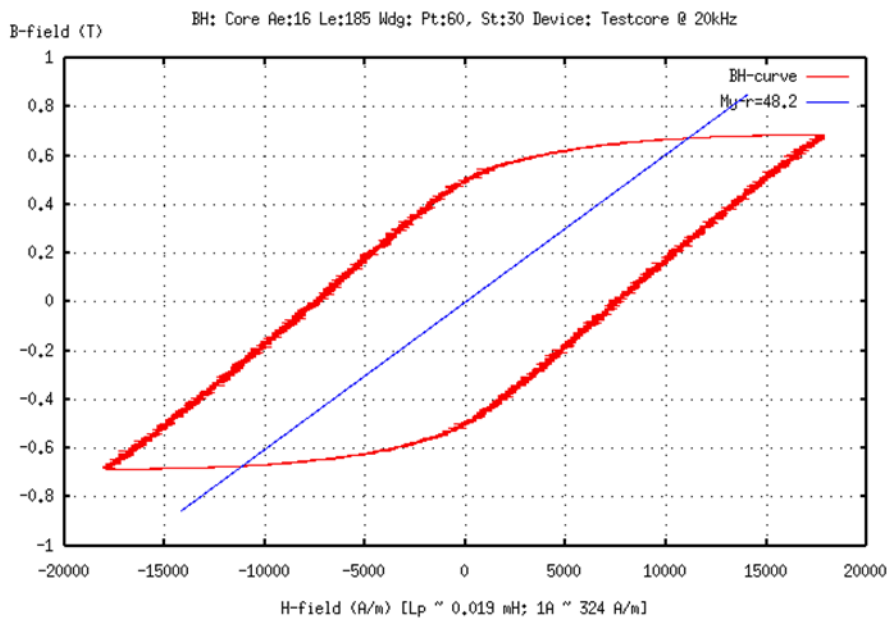


Figure 9. The BH-curve for A9 obtained at 20 kHz

If we calculate the applied dB/dt in the figure above the flux goes from almost from -0.7T to +0.7T and then back to -0.7T in 50 μ s (one period at 20 kHz). So, 2.8T / 50 μ s = 0.056 T/ μ s. A measurement at 50 kHz was not possible due to core heating too quickly.

When trying to measure the B9 and C9 cores they heated up so quickly that the insulation failed before any measurement was captured. The C9 core was rewound with a 30turns softer multi-stranded wire. Unfortunately, the core broke in several places while removing the old wiring, so it was remeasured at low and medium currents at 50 Hz to see if still measured OK. The result was that permeability decreased from 163 to 150 at low current and from 142 to 135 at medium current which is expected due to the small air-gaps introduced due to the core breaking. Also, the coercivity decreased, in this case from 227 to 175 A/m at low current and 514 to 366 A/m at medium current which is not explained by the air-gaps. A BH curve at lower current was then obtained at 20 kHz for the C9 core, see Figure 10.

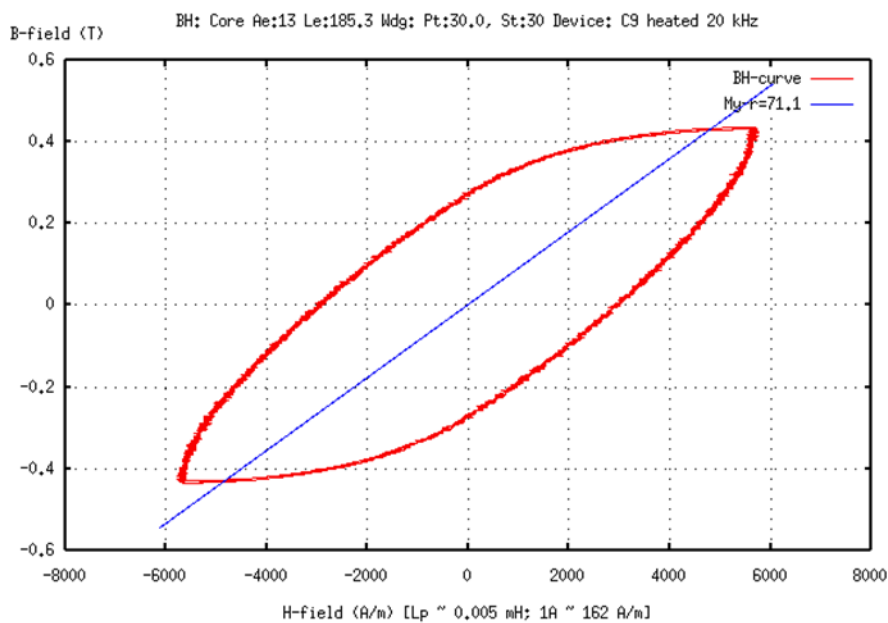


Figure 10. A BH curve for the C9 core.

It is hard to see if this is better than the A9 material. If so it is probably mostly due to that the core thickness was reduced to 2.51 mm from 3.20 mm, which reduces the eddy-current losses.

Resistivity and eddy current losses

Resistance of ½ circumference (92.6 mm) of the test core was measured to 22.5mΩ. This gives a resistivity of 3.89E-6Ωm. This is far too low for a core that is not laminated. The B9 and C9 cores were measured in a similar way.

Sample	Measured resistivity (Ωm)
B9 Untreated	3.89E-6
B9 Heat treatment B	3.76E-6
C9 Heat treatment C	3.62E-6

To give a rough understanding of the problem – consider a rectangular tube (marked in red in figure below) that is 35 mm long and has a wall thickness of 1 mm. The circumference of the tube is 21+17+21+17 mm = 76 mm. The area is 35mm². The resistance around one turn is $3.89E-6 * 0.076 / 35E-6 = 8.4m\Omega$.

If we want to design a transformer with the mentioned core that gives an output voltage of 10V/turn the losses in this sheet only would be $U^2/R = 10^2 / 0.0084 = 11.9 \text{ kW}$.

Conclusions - Magnetic measurements

As is, this material is not suitable for high frequency inductors or transformers.

The tested heat-treated samples did not produce any significant improvement to change the above conclusion.

5 3D printed E-core

An E-core inductor was 3D-printed by Exmet, according to the drawing in Figure 11, see also Figure 12. The E-core inductor was not evaluated, since the solid geometry of the present FeSiB alloy resulted in a too high eddy current.

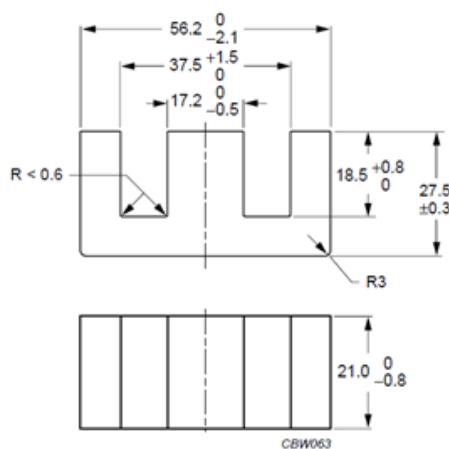


Figure 11. Design drawing of the E-core inductor

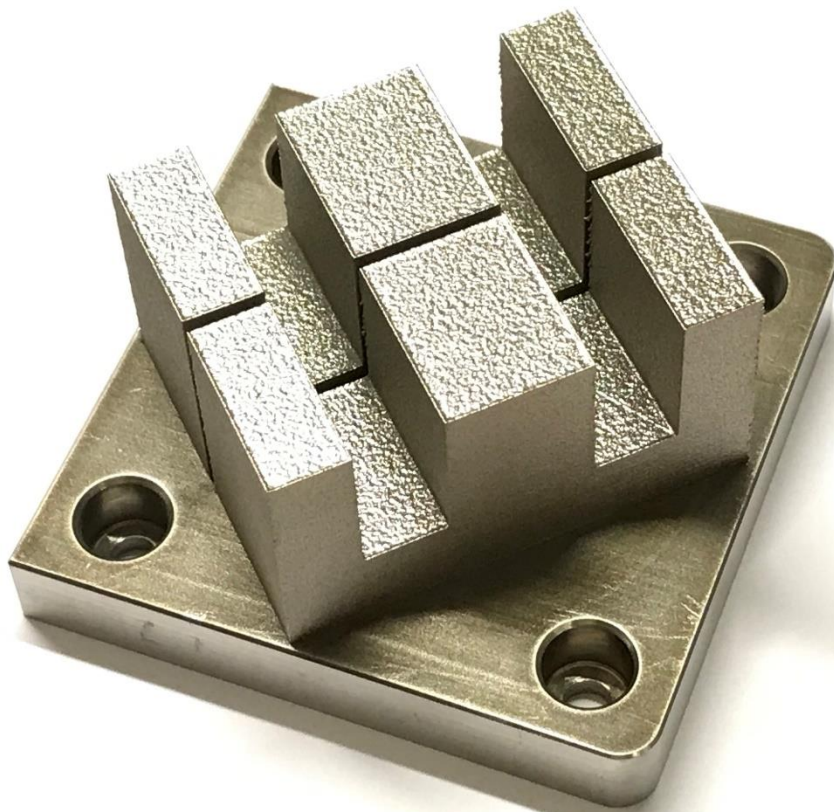


Figure 12. The 3D-printed E-core inductor.

6 Discussions

Soft magnetic materials are the materials that can rapidly switch their magnetic polarization under a small, applied field. Permeability, magnetic flux density, and intrinsic coercivity are the key figures of merit in DC applications. In AC applications, the soft magnetic materials are magnetized and demagnetized repeatedly following the frequency of the alternating current supplied to the induction coil. Transformers, generators, and electric machines are all operated in AC conditions. In addition to sufficient magnetic flux density, minimum energy loss is the most important consideration in AC applications. [1]

The difference between inductor and transformer is that inductors handle a small amount or ripple current but a large average current, while a transformer typically has a high alternating current but zero average current [2].

There are three general types of materials used for inductor magnetic cores: powder cores comprised of various iron alloys, ferrites, and wound cores comprised of thin magnetic steel strips. Of these, the most common materials are ferrites for transformers, iron-powder for inductors.

6.1 Methods to reduce the eddy current

In this study a 3D printed amorphous/nanocrystalline solid core aimed for an E-core inductor was evaluated. The target value of permeability was not reached but could still be used for an inductor. However, the losses were too high mainly due to the eddy current. There are three ways to reduce the eddy current that may be considered:

- 1) 3D printed internal structure to break up the eddy current
- 2) Coat each powder-particle with an insulating layer. The layer needs also act as a binder/adhesive to keep the inductor together
- 3) A laminated structure with insulating layer in-between each layer.

A more detailed description of the three alternatives is presented in the text below.

3D printed internal structure to break up the eddy current

Plotkowski, et al. have demonstrated that a 3D printed internal structure of the core could reduce the eddy current. The most efficient structure was a novel Hilbert curve design, see *Figure 13*. However, the structure influences the heat transfer characteristics of the process and the resulting microstructure [3].

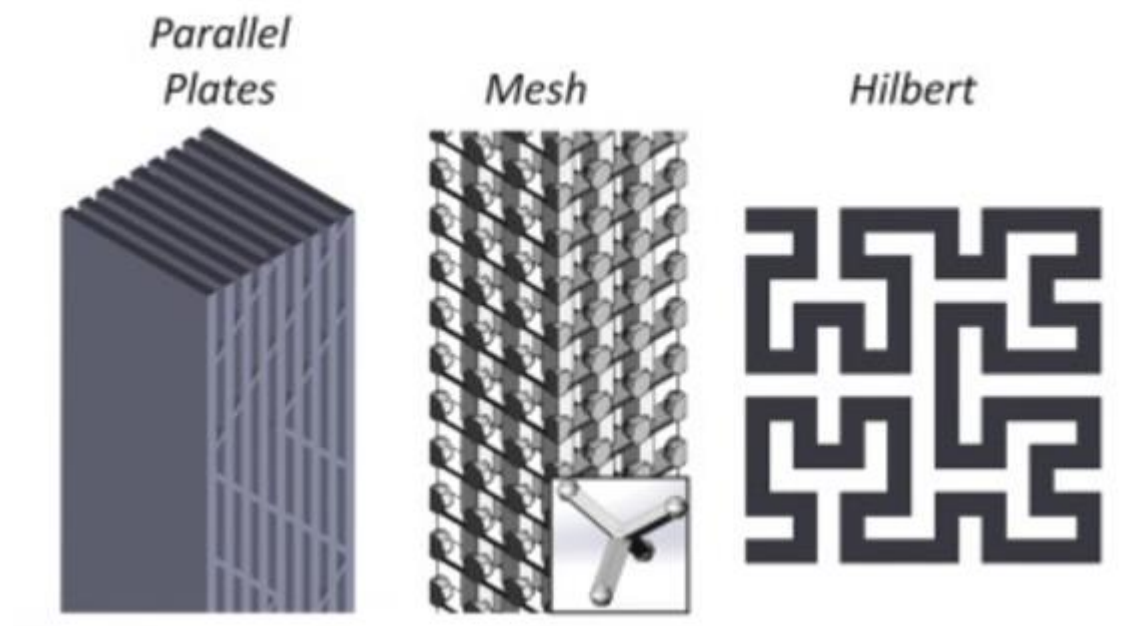


Figure 13. Examples of internal structures to reduce the eddy current for 3D printed soft magnetic cores [3].

Coat each powder-particle with an insulating layer

Powder cores consist of fine particles and are coated with an insulating layer. The insulating coating can be organic or inorganic, where the organic coatings typically are epoxy, acrylic, polyester, epoxy-polyester hybrid, and polyurethane, and the inorganic coating can be an oxide (such as Fe_2O_3), a phosphate (such as zinc phosphate, iron phosphate, and manganese phosphate) [4]. Silica coating can also be used, and it provides excellent stability against corrosion, oxidation, and has a high thermal-resistance [5].

The manufacturing of $\text{Fe}_{73.5}\text{Cu}_1\text{Nb}_3\text{Si}_{15.5}\text{B}_7$ (at. %) amorphous powder coated with an insulating layer has been described by Jiang, X Li et.al [6]. The insulating layer consisted of an organic binder (cyanate resin solution diluted by acetone) and an inorganic binder (glass powder). The prepared cores were annealed at 480°C to relieve the stress and 580°C to form nanocrystalline structure.

Pure iron powder with an insulating layer on the surface can be achieved by treating the powder with aqueous phosphoric acid to produce phosphate insulating layer on the surface. After drying the powder, the powder should be mixed with 0.5wt% Zn stearate and compacted in a mold with a diameter of 20mm at 800MPa. The powder compacts were then heat treated at 500°C for 1 hour. The results showed that insulated iron powder was obtained with uniform phosphate layer by chemical reaction. With increased amount of phosphate layer, the core loss and density of compacts were decreased [7].

A laminated structure with insulating layer in-between each layer

A laminated structure with insulating layer in-between each layer is the traditional approach to reduce the eddy current. The resulting product is a stack of thin laminates insulated from each layer.

6.2 Material properties

The development trend of soft magnetic materials is depicted in *Figure 14. Development trend of soft magnetic materials []*

according to C. Jiang et.al [8]. Fe-based Nano alloys may at present best fulfill the requirement of both small size and low energy loss.

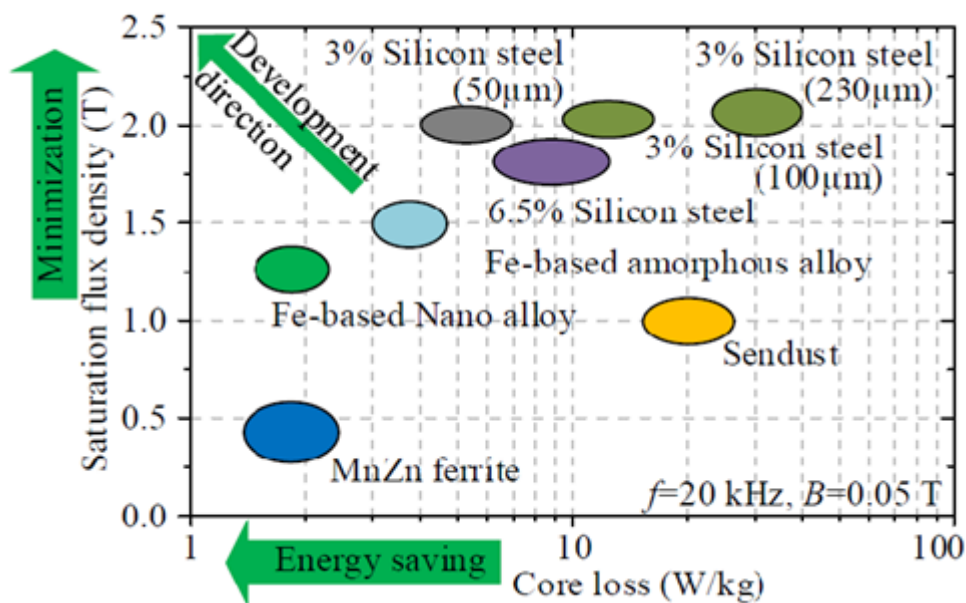


Figure 14. Development trend of soft magnetic materials [8]

The required performance of the material in this study was as follows:

- dB/dt between 0.1 T/μs to 0.2 T/μs without excessive losses.
- Saturation flux minimum 0.3 T
- Saturation flux preferred > 0.6 T
- Permeability minimum 500
- Permeability preferred > 1000

According to a review made by Chaoqiang Jiang et.al [9] the only material that fulfil the requirements are Fe-Ni-Mo (product name MPP). Therefore, it would be interesting in a future work to evaluate the magnetic properties of a toroid made of the Fe-Ni-Mo alloy.

Table 5. Magnetic material properties from several manufactures [9].

TABLE. II MAGNETIC MATERIAL PROPERTIES FROM SEVERAL MANUFACTURERS					
Manufacturer	Product name	Material composition	Saturation flux density B_{sat} [T]	Curie temperature T_c (°C)	Relative permeability μ_r
AT&M Corp.	MGMP	Fe-Cu-Nb-Si-B	1.0	570	60
Magnetics	Kool Mμ	Fe-Al-Si	1.0	500	14-125
Magnetics	XFlux	Fe-Si	1.6	700	26-90
Magnetics	High Flux	Fe-Ni	1.5	500	14-160
Magnetics	MPP	Fe-Ni-Mo	0.8	460	14-550
Magnetics	Amoflux	Fi-Si-B	1.5	400	60
CSC	Sendust	Fe-Al-Si	1.0	500	26-125
CSC	Mega Flux	Fe-Si	1.6	700	26-90
CSC	High Flux	Fe-Ni	1.5	500	26-160
CSC	MPP	Fe-Ni-Mo	0.7	450	14-200
Micrometals	Mix-52	Fe	1.85	<770	75

7 Project goal

The goal was to evaluate high-frequency 3D-printed inductor with optimized soft magnetic properties. The opportunity to mass produce 3D-printed inductors should also be examined.

8 Results and goal fulfillment

The goal was to evaluate a 3D printed inductor with optimized properties for high frequencies, which was done within the project. The project increased knowledge of using 3D-printed amorphous / nanocrystalline materials for inductors and transformers, and it provided a basis for further development.

The project also involved a collaboration between a university (KTH), Institute (Swerim), SME companies (Exmet) and OEM (Inmotion), which contributes to a competitive research and innovation environment in Sweden. For Exmet, this meant that important material data were obtained for Exmet's first commercial powder which was launched after the project.

A soft magnetic powder material that met Inmotion's requirements specification was found during the project work, this is important as it can be a reference for further development, or the powder material may be partly or wholly included in future inductors. The project may thus contribute to the development of energy-efficient drive systems for electric vehicles. With more efficient electric vehicles, fossil dependence will be reduced, which is in line with Future technical development stated in the FFI Roadmap for Electronics for "Green, safe, autonomous and connected functions", sub-area "Electronics for energy efficient, safe and connected functions".

9 Dissemination and publication

9.1 Dissemination of knowledge and results

How will the project results be used and disseminated?	Mark with X	Comments
Increase knowledge in the field	X	
Passed on to other advanced technical development projects	X	
Passed on to product development projects		
Introduced to the market	X	Material properties was obtained for Exmet's first commercial product, amorphous/nanocrystalline FeSiB type alloy (metal powder)
To be used in investigations / regulations / permit matters / political decisions		

9.2 Publikations

Swerim Report 102251

10 Conclusions and further research

Based on the evaluation of 3D printed test samples of amorphous/nanocrystalline FeSiB type alloy, the following conclusions are due:

4. The present design with a solid core resulted in a too high eddy current.
5. The present type of alloy amorphous/nanocrystalline FeSiB type alloy may result in both small size of the inductor and low losses, according to a reference [8].
6. Only one material was found in the literature that fulfilled the required properties of the soft magnetic material [9].

Exmet, Inmotion and Swerim are in discussion to continue the research.

11 Project participants and contact persons

Lars Lindberg	Inmotion Technologies AB
Mattias Unosson	Exmet
Hans Peter Nee	KTH
Tag Hammam	Swerim

12 Acknowledgments

This investigation was funded by Inmotion Technologies AB, Exmet and Vinnova, within the program "Fordonstrategisk Forskning och Innovation", FFI . Members of the research committee from the industry were

Thord Nilson and Lars Lindberg, Inmotion Technologies

Mattias Unosson and Lena Thorsson, Exmet

Who are greatly acknowledged

13 References

- ¹ Gaoyuan Ouyang, Xi Chen, Yongfeng Liang, Chad Macziewski, Jun Cui, Review of Fe-6.5 wt%Si high silicon steel—A promising soft magnetic material for sub-kHz application, *Journal of Magnetism and Magnetic Materials*, Volume 481, 2019, Pages 234-250,
- ² <https://www.powerelectronicstips.com/comparing-magnetic-cores-for-power-inductors-faq/>
- ³ Plotkowski, A., Pries, J., List, F., Nandwana, P., Stump, B., Carver, K., & Dehoff, R. R. (2019). Influence of scan pattern and geometry on the microstructure and soft-magnetic performance of additively manufactured Fe-Si. *Additive Manufacturing*, 29, 100781. <http://doi.org/10.1016/j.addma.2019.100781>
- ⁴ Review of Fe-6.5 wt%Si high silicon steel—A promising soft magnetic material for sub-kHz application, *Journal of Magnetism and Magnetic Materials*, Volume 481, 2019, Pages 234-250, ISSN 0304-8853,
- ⁵ Ishizaki, T.; Nakano, H.; Tajima, S.; Takahashi, N. Improving Powder Magnetic Core Properties via Application of Thin, Insulating Silica-Nanosheet Layers on Iron Powder Particles. *Nanomaterials* 2017, 7, 1.
- ⁶ C. Jiang, X. Li, S. S. Ghosh, H. Zhao, Y. Shen and T. Long, "Nanocrystalline Powder Cores for High-Power High-Frequency Power Electronics Applications," in *IEEE Transactions on Power Electronics*, vol. 35, no. 10, pp. 10821-10830, Oct. 2020, doi: 10.1109/TPEL.2020.2979069.
- ⁷ Cha, Hyun Rok, et al. "Insulation and Magnetic Properties of Iron Powder Coated by Wet Chemical Method." *Materials Science Forum*, vol. 534–536, Trans Tech Publications, Ltd., Jan. 2007, pp. 1329–1323.
- ⁸ C. Jiang, X. Li, S. S. Ghosh, H. Zhao, Y. Shen and T. Long, "Nanocrystalline Powder Cores for High-Power High-Frequency Power Electronics Applications," in *IEEE Transactions on Power Electronics*, vol. 35, no. 10, pp. 10821-10830, Oct. 2020, doi: 10.1109/TPEL.2020.2979069.
- ⁹ Jiang, C. et al. "Nanocrystalline Powder Cores for High-Power High-Frequency Power Electronics Applications." *IEEE Transactions on Power Electronics* 35 (2020): 10821-10830.